Available online at www.sciencedirect.com

jmr&t Journal of Materials Research and Technology

www.jmrt.com.br

Original Article

Effect of glycerol on EDLC characteristics of chitosan:methylcellulose polymer blend electrolytes

Shujahadeen B. Aziz[a,b,*], *M.H. Hamsan*[c], *M.A. Brza*[a,e], *M.F.Z. Kadir*[f], *S.K. Muzakir*[g], *Rebar T. Abdulwahid*[a,d]

[a] *Advanced Polymeric Materials Research Lab., Department of Physics, College of Science, University of Sulaimani, Qlyasan Street, Sulaimani, Kurdistan Regional Government, Iraq*

[b] *Department of Civil engineering, College of Engineering, Komar University of Science and Technology, Sulaimani 46001, Kurdistan Regional Government, Iraq*

[c] *Institute for Advanced Studies, University of Malaya, 50603 Kuala Lumpur, Malaysia*

[d] *Department of Physics, College of Education, University of Sulaimani, Old Campus, Sulaimani 46001, Kurdistan Regional Government, Iraq*

[e] *Manufacturing and Materials Engineering Department, Faculty of Engineering, International Islamic University of Malaysia, Kuala Lumpur 50603, Gombak, Malaysia*

[f] *Centre for Foundation Studies in Science, University of Malaya, Kuala Lumpur 50603, Malaysia*

[g] *Material Technology Program, Faculty of Industrial Sciences & Technology, Universiti Malaysia Pahang, Lebuhraya Tun Razak, Gambang, Kuantan 43600, Pahang, Malaysia*

ARTICLE INFO

Article history:
Received 7 April 2020
Accepted 26 May 2020

Keywords:
Polymer blend electrolyte
Glycerol plasticizer
Natural polymers
Impedance spectroscopy
XRD analysis
EDLC study

ABSTRACT

Chitosan (CS):methylcellulose (MC):NH_4I based solid polymer electrolyte (SPE) has been plasticized using glycerol due to its hydroxyl-rich structure. All SPEs are prepared using solution cast technique at room temperature. Prior to device application, structural, electrical and electrochemical characteristics were examined for the prepared samples using various techniques. X-ray diffraction (XRD) investigation was used to explain the structural changes. Electrical impedance spectroscopy (EIS) was used to evaluate the DC conductivity. The potential stability of the highest conducting film (6.65×10^{-4} S cm^{-1}) was found to be 2.2 V as well as shows the characteristic of an ionic conductor where $t_{ion} > t_e$. The layers of the electrical double-layer capacitor (EDLC) consist of two identical activated carbon electrodes sandwiching the highest conducting SPE. The existence of charge double-layer in the fabricated EDLC has been verified using cyclic voltammetry test. From galvanostatic charge–discharge measurements, several crucial EDLC parameters have been obtained, e.g. specific capacitance, internal resistance, energy density and power density. The addition of glycerol improved the performance of the EDLC.

* *Corresponding author.*
E-mails: shujaadeen78@yahoo.com, shujahadeenaziz@gmail.com (S.B. Aziz).

https://doi.org/10.1016/j.jmrt.2020.05.114

1. Introduction

The recipe to fabricate solid-state energy devices usually consists of electrodes and electrolyte. To produce high performance energy devices, e.g. fuel cells, batteries, sensors and electrochemical capacitors, the conductivity value of the electrolyte should be more than 10^{-4} S cm^{-1} [1]. Polymer electrolytes are membrane consisting of organic or inorganic salts dissolved in a polymer. Different biopolymers can be used as a hosts for ionic conduction such as zwitterionic, poly(ethylene oxide) (PEO), poly(ethylene glycol), poly(vinyl alcohol) (PVA), methylcellulose and dextran [2–8]. Generally, biopolymers are abundant, cheap, eco-friendly and may replace synthetic polymers for use in energy generation and storage devices. Recently, biopolymer based electrolytes have been investigated extensively and employed as both the electrolyte and separator in EDLC and energy storage devices [9–13]. Since polymer electrolytes must function as both the electrolyte and separator in a many devices, they must have good electrochemical and thermal stability, sufficient conductivity and chemically and electrochemically compatible with the electrode materials [14].

Several methods have been proposed to improve the DC conductivity, for instance polymer blending, salt doping, polymer grafting, inclusion of nanofiller and plasticization [15]. Plasticization is where plasticizer is added to the polymer matrix. Typically, unplasticized SPE is rigid due to strong interaction between polymers. Hence, the presence of plasticizer can reduce the attractive forces among polymer chains, which make them more flexible [16]. Mattew et al. [17] reported that the crystallinity and glass transition temperature of polyethyl methacrylate:$LiClO_4$ reduced with the inclusion of plasticizer. Glycerol is a non-toxic compound with high boiling point (290 °C) as well as low melting point (18 °C), which avoids the vaporization and solidification process at ambience temperature [18]. The chemical formula of glycerol ($C_3H_8O_3$) portrays that glycerol has a multihydroxyl moiety structure, meaning that more electron lone pairs are available for ionic conduction. The high value of glycerol dielectric constant (42.5) enhances salt dissociation as well as decreases the polymer–polymer interactions [19].

Protonic-based energy devices are one of the options to replace the convention of lithium-based energy devices. This is due to small ionic radius of H^+ ion (0.84×10^{-15} m) compared to that of Li^+ (0.90×10^{-10} m) [20]. Two common protonic sources are strong inorganic acid and ammonium-based salt. Rosi et al. [21] reported a SPE system based on polyvinyl alcohol:hydroxyethylcellulose doped with sulphuric acid (H_2SO_4). As reported by Łatoszynska et al. [22], phosphoric acid (H_3PO_4) possesses a conductivity of $\sim 10^{-4}$ S cm^{-1} with a low activation energy. However, inorganic acid-based SPE suffers from chemical degradation as well as poor mechanical integrity [23]. Ammonium salts have been reported as proton provider in many biopolymer electrolyte systems [24–26]. According to Shuhaimi et al. [27], the responsible charge carriers in CS:κ-carrageenan:NH_4NO_3 system is the H^+ ion. Cation from ammonium salt is NH_4^+, where one of the H^+ ions possesses the weakest bond, which can be easily separated under influence of electric field. This free H^+ ion hops from one site to another and this process is called Grotthuss mechanism [28].

Electric double-layer capacitors (EDLCs) are well known to be the support energy system in hybrid electrical vehicles due to their high power density, long life cycle and rapid charge–discharge rate [29]. Carbon-based electrodes have gained interest from energy related applications because of their chemical and thermal stability as well as abundance. Activated carbon is essentially indicated as carbonaceous material with high physical and chemical stabilities, high porosity and large surface area [30]. Activated carbons are used as active material in the electrodes because they have excellent conductivity, pore volume ~0.5 cm^3 g^{-1}, surface area more than 1000 m^2 g^{-1} and relatively low cost [31]. Thus, in this work CS has been blended with MC as the polymer host. NH_4I has been chosen as the proton provider due to its low lattice energy of 605.3 kJ mol^{-1}. Low lattice energy salt is easier to dissociate compared to the one with high lattice energy [32]. EDLC based on unplasticized CS:MC:NH_4I has been reported previously in our work [33]. The main focus of this study is to enhance the conductivity and amorphousness of the CS:MC:NH_4I electrolyte by addition of glycerol and fabricate an EDLC using the highest conducting CS:MC:NH_4I:glycerol. The performance of EDLC in this study is superior compared with the unplasticized system.

2. Experimental methods

2.1. Materials

Methylcellulose (MC) (4000 cP), chitosan (CS) (310,000–375,000 g mol^{-1}) and low molecular weight glycerol plasticizer were supplied by Sigma–Adrich. Carbon black, N-methyl-2-pyrrolidone (NMP) and ammonium iodide (NH_4I) were obtained from Timcal, EMPLURA and HmbG chemicals, respectively. Activated carbon (RP20) and polyvinylidene fluoride (PVdF) were supplied by magna value company.

2.2. Electrolyte preparation

30 wt.% MC and 70 wt.% of CS were dissolved in 40 mL of 1% acetic acid separately for the CS:MC polymer blend preparation at ambient temperature for around 3 h. Subsequently, the solutions were combined and stirred for extra 2 h until a homogeneous solution was achieved. Consequently, a fixed amount of NH4I (40 wt.%) was added to the CS:MC solutions separately to prepare polymer blend electrolyte solutions. The CS:MC:NH_4I polymer blend solutions were plasticized with different concentrations of 5, 10, 15 and 20 wt% glycerol to produce plasticized polymer blend electrolyte films. The prepared samples were coded as CSMC1, CSMC2, CSMC3, and CSMC4, for CS:MC:40 wt.%NH_4I system incorporated with 5, 10, 15, and 20 wt% glycerol plasticizer, respectively. The solutions were reserved in the plastic Petri dishes and then left for drying at ambient temperature. For drying further, the synthesized films were kept in a dessicator including silica gel before characterizations.

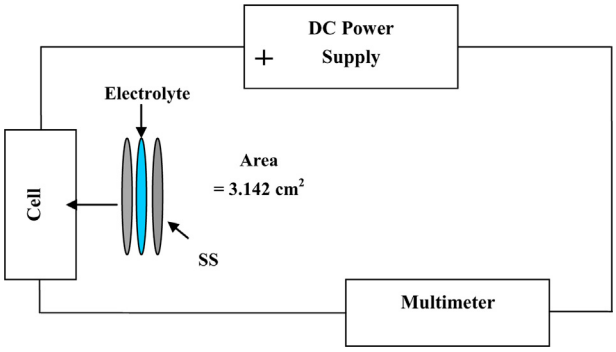

Fig. 1 – Illustration of TNM analysis circuit setup.

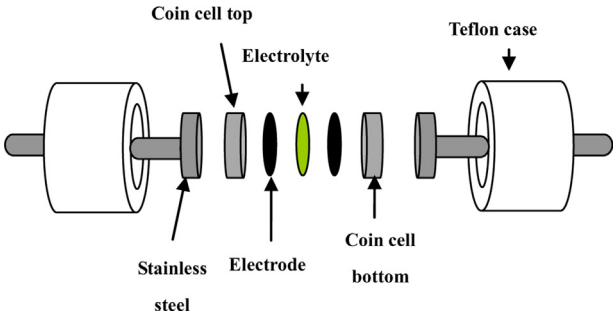

Fig. 2 – Illustration of fabricated EDLC.

2.3. *Characterization techniques*

X-ray diffraction (XRD) patterns were accomplished using Empyrean X-ray diffractometer (PANalytical, Netherland) with operating current and operating potential of 40 mA and 40 KV, respectively. The samples were scanned with a monochromatic CuKα X-radiation beam at the wavelength of (λ = 1.5406 Å) as well as the glancing angles (2θ) of the X-ray diffraction was in the range from 5° to 80° using a step size of 0.1°.

The impedance spectra of the samples were achieved using HIOKI 3531 Z Hi-tester in the frequency range from 50 Hz to1000 kHz. The films were cut into small discs (diameter = 2 cm) and then they were placed between the two stainless steel (SS) electrodes under spring pressure. The cell was attached to a computer equipped with a software to calculate the real (Z′) part and the imaginary (Z″) part of the complex impedance (Z*) spectra.

2.4. *Electrolyte characterization*

2.4.1. *Transference number measurement (TNM) study*

Two types of transference number (TNM) were investigated, i.e. ionic (t_{ion}) and electronic (t_e) TNM. The cell arrangement was stainless steel|highest conducting sample (CSMC4)|stainless steel. The cell was connected to a UNI-T UT803 multimeter and V&A Instrument DP3003 digital DC power supply. The circuit for TNM setup is shown in Fig. 1. The operating voltage was 0.2 V, where the cell was polarized versus time at room temperature. t_{ion} can be obtained from the following equation:

$$t_{ion} = \frac{I_i - I_{ss}}{I_i} \quad (1)$$

Here, initial and steady-state current are denoted as I_i and I_{ss}, respectively. The total of t_e and t_{ion} is equal to 1, that is, $t_e = 1 - t_{ion}$.

2.4.2. *Linear sweep voltammetry (LSV)*

Before fabrication of energy devices is done, linear sweep voltammetry (LSV) analysis was performed to check the potential stability of the electrolyte (CSMC4). The cell arrangement for LSV was the same with TNM analysis. Scan rate of 100 mV s^{-1} was used from 0 to 4 V at room temperature. The cell was connected to working, reference and counter electrodes using Digi-IVY DY2300 potentiostat. The changes in current value at working electrode was monitored, while potential was sweep linearly between working and counter electrodes.

2.5. *Activated carbon electrode preparation*

The active electrode material used was activated carbon (3.25 g) from Kuraray and electronic conductor was carbon black (0.25 g) from Magna Value. The surface area of activated carbon based on the specification by Kuraray was 2500 m^2 g^{-1}. These powders were grinded in a planetary ball miller at 500 r min^{-1} for 20 min. An amount of 0.5 g polyvinylidene fluoride (PVdF) was dissolved in 15 mL of N-methyl-2-Pyrrolidone (NMP) for few hours. The grinded powders were then added to the NMP-PVdF solution and stirred for 2 h until black thick solution was obtained. This activated carbon solution was coated on an aluminum foil using a doctor blade, which was pre-washed with acetone. The electrode was left to dry in an oven at 60 °C.

2.6. *EDLC fabrication and characterization*

The electrode was cut into a circle shape with area of 2.01 cm^2. The highest conducting electrolyte (CSMC4) was sandwiched between two electrodes and placed in a CR2032 coin cell. This coin cell then was mounted in a Teflon case, as shown in Fig. 2.

Digi-IVY DY2300 potentiostat was used to conduct cyclic voltammetry (CV) of the EDLC. The EDLC shown in Fig. 2 was subjected to a scan rate of 0.01 V s^{-1} from 0 to 0.9 V. The specific capacitance (C_{cv}) of the EDLC can be obtained from the CV plot via the following equation:

$$C_{cv} = \int_{V_i}^{V_f} \frac{I(V)\,dV}{2ma\left(V_f - V_i\right)} \quad (2)$$

Area of the CV plot $\int (I(V)dV)$ can be obtained from integration function in Origin 9.0 software. a is the scan rate, m stands for mass of activate material, while V_f and V_i are the final (0.9 V) and initial voltage (0 V), respectively. The rechargeability of the EDLC is tested using NEWARE battery cycler for 100 complete cycles at a current density of 0.4 mA cm^{-2}. The environment to test the charge–discharge and CV of the EDLC was regulated at relative humidity ~50% and temperature ~25 °C.

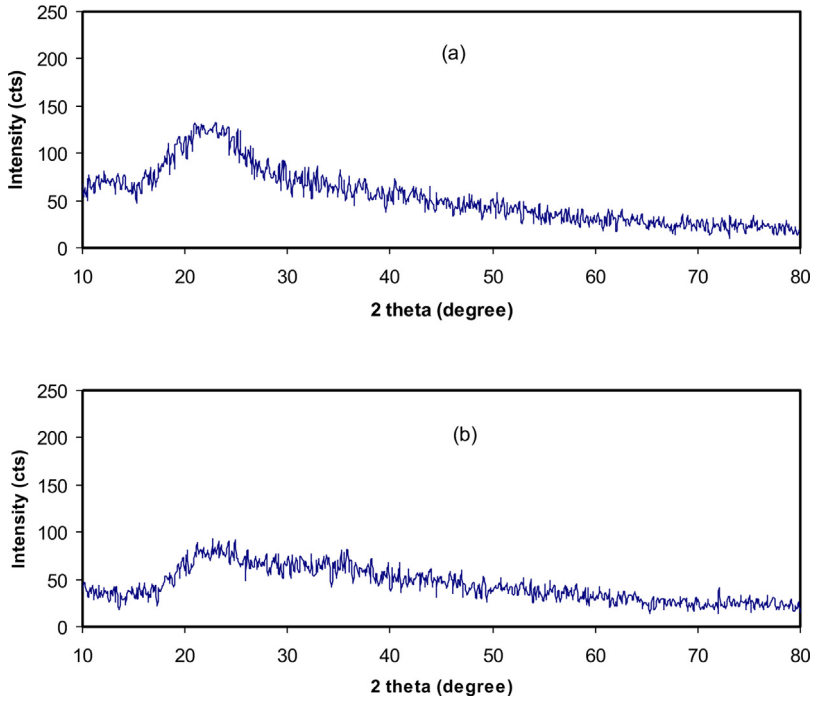

Fig. 3 – XRD spectra of (a) CSMC2 and (b) CSMC4 electrolyte films.

The specific capacitance (C_d) from discharge curve can be calculated from the following equation:

$$C_d = \frac{i}{xm} \tag{3}$$

where i is the applied current and x is the gradient of discharge part. The value of C_{cv} and C_d of the EDLC will be compared to check the consistency of the results. The cyclability and condition of electrode–electrolyte contact of the EDLC was verified using the following equation:

$$R_e = \frac{V_{drop}}{i} \tag{4}$$

where R_e is the equivalent series resistance and V_{drop} is the potential drop before discharging process.

3. Results and discussion

3.1. *Structural study*

Fig. 3(a and b) illustrates the XRD patterns of CS:MC:NH_4I glycerolized with 20 wt.% and 40 wt.% of glycerol plasticizer. Earlier reports designated that MC host polymer possesses a peak at $2\theta = 9–21^\circ$, which rises from the small-distance order in the MC polymer chains as well as the intermolecular hydrogen bonding [34–36]. In contrast, pure chitosan semi-crystalline structure is confirmed by a variety of earlier studies [37,38]. Chitosan possesses various crystalline peaks around $2\theta^\circ = 5^\circ$ and 20°, which is essentially owing to the crystalline structure of the average intermolecular distance of the chitosan membrane [39,40]. The inter- and intra-molecular hydrogen bonding developed among the amino group and hydroxyl group throughout an absorbed molecule of water provides a compact crystalline composition to the chitosan [41,42]. In our prior study [33], it was found that inclusion of 40 wt.% of NH_4I salt to CS:MC system develops the broadening hump in the CS:MC system. The cause behind the crystallinity reduction is because of the inclusion of the ammonium salt to the CS:MC polymers [33]. Additionally, the complex development among the cations of the ammonium salt and the functional groups of the polymer as a result of the electrostatic interactions and disturbing molecular hydrogen bonding increased the amorphous region [33]. It is noticeable that upon the insertion of the plasticizer the widening of the peak is more enlarged (see Fig. 3a and b) in comparison with the unplasticized CS:MC:NH_4I electrolyte system in our previous work [33]. This decrease in crystallinity may be associated to the molecular hydrogen bonding destruction and more salts dissociation in the electrolyte system [16–19]. It is documented that the glycerol monomer possesses three hydroxyl (OH) functional groups [19], and as a result it hinders the crystalline composition order inside the polymer electrolyte as a result of disturbing molecular hydrogen bonding. Both reduction in intensity and widening in peak indicate that the amorphous component inside the polymer blend is a main. An additional benefit of XRD examination is that it can be employed to expect the trend of conductivity of the electrolytes system [43]. The XRD analysis and AC impedance investigation can be mixed to clarify the conductivity variation with the concentration of plasticizer. The analysis indicates that the amorphous phase of the sample enhances with raise in glycerol concentration. The enhancement in the amorphous component lead to a diminution in the energy barrier to the polymer electrolyte segmental motion. H^+ ions hopping from one polymer

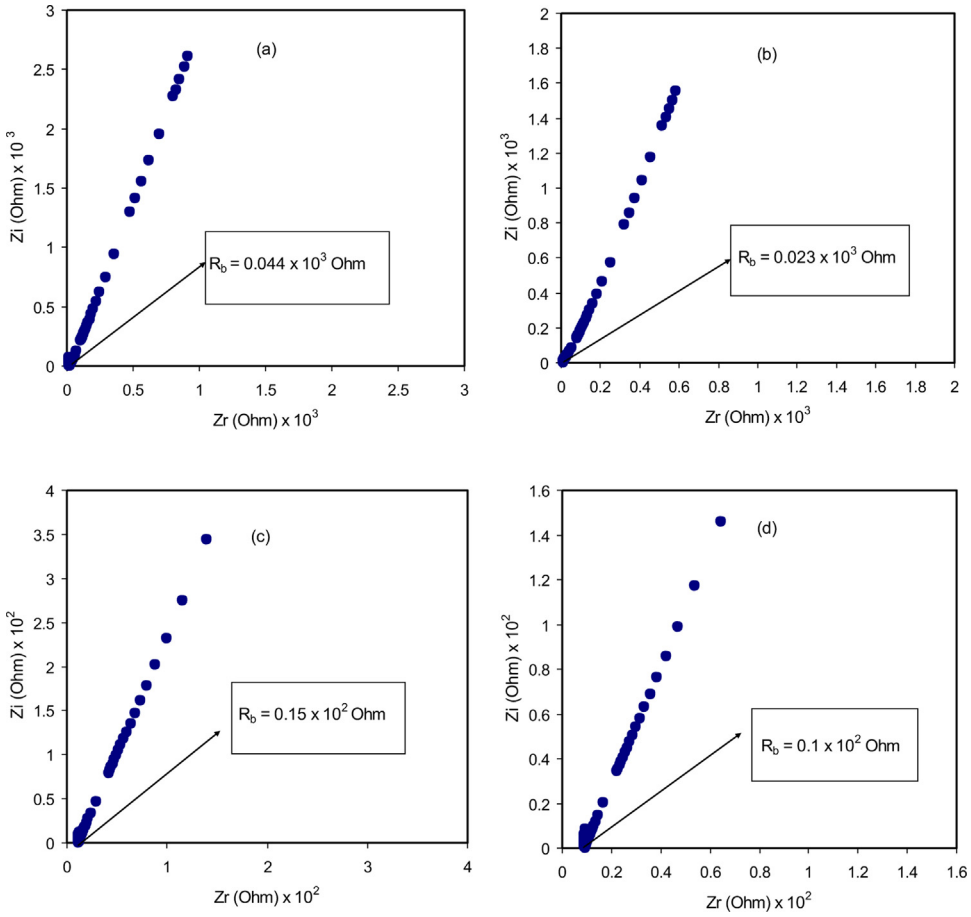

Fig. 4 – Impedance plot for (a) CS:MC1, (b) CSMC2, (c) CSMC3 and (d) CSMC4.

segment to another is more assisted by the occurrence of a liquid-like environment offered by the glycerol.

3.2. *Impedance study*

Polymer electrolyte is the interesting matter in the advanced materials area for application in devices. Rapid ion migration takes place in polymer electrolytes over glass transition temperature [44]. Earlier investigations indicated that ion migration in polymer electrolytes enhances through the inclusion of plasticizers with low molecular weight [45]. Impedance spectroscopy is an influential technique for investigating the electrolyte materials electrical properties and the interfaces between the electrolytes and electronically conducting electrodes [46]. Fig. 4(a–d) shows the impedance plots for the CS:MC:NH_4I:glycerol system. The ideal impedance spectra for the resistor and capacitor parallel connection must be a normal semicircle with having a diameter-matched with the real axis [47]. Typically, complex impedance plots indicate two distinct regions: the semicircle at the high frequency region, which is by reason of the electrolytes bulk effect, and the spike or tail at the low frequency region, which is owing to the blocking electrodes effect [46]. The high frequency semicircle gives details regarding the electrolyte properties for example bulk resistance (R_b) and bulk capacitance (C), which stem from the ions transportation and the dielectric polarization in polymers, correspondingly [48]. The missing of semicircular region at the high frequency region points out that the conduction is essentially owing to the ions. The spike is seen at the low frequency region as a result of the electric double-layer capacitance at the blocking electrodes [49,50]. It is clear that upon the inclusion of the plasticizer the semicircles at the high frequency region are absent (see Fig. 4a–d), while the semicircles were observed in the unplasticized electrolyte system of CS:MC incorporated with 10, 20 and 30 wt.% NH_4I in our previous work [33]. From earlier report [51], the inclusion of 30 wt% ammonium nitrate (NH_4NO_3) in the potato starch (PS)-MC polymer blend produced the conductivity of $4.37 \pm 0.16 \times 10^{-5}$ S cm^{-1}. In the current study, the DC conductivity of the electrolyte system improves to 6.65×10^{-4} S cm^{-1} with 40 wt.% of glycerol. The point where the semi-circle intercepts the real axis (Z) offers the bulk resistance (R_b) value. By considering the R_b value as well as the sample dimensions, the film conductivity can be computed using the relation,

$$\sigma_{dc} = \left(\frac{1}{R_b}\right) \times \left(\frac{t}{A}\right) \quad (5)$$

where l, R_b, and A represent the thickness, bulk resistance and area of the electrolyte sample, respectively. This idea was supported in the sense that the electrical conductivity relies on

Table 1 – Achieved DC conductivity of the plasticized CS:MC:NH_4I electrolyte systems.

Sample designation	DC conductivity ($S\,cm^{-1}$)
CSMC1	1.56×10^{-4}
CSMC2	2.98×10^{-4}
CSMC3	4.56×10^{-4}
CSMC4	6.65×10^{-4}

the charge carrier number density as well as carrier mobility, as follows [7]:

$$\sigma = \sum \eta q \mu \tag{6}$$

Here η denotes the charge carrier density, q denotes to the typical meaning (1.6×10^{-19} C), and μ denotes the mobility of ion.

From earlier study it is confirmed that the charge carrier species in the system of the polymer/ammonium salt is the H^+ ion supplied by ammonium ion [52]. The mainly general method of proton conduction is structure diffusion, which is known as Grotthuss mechanism, where exchanging of the ions takes place among the complexed sites [53]. Proton conduction through the Grotthus mechanism is explained considering that the proton makes a jump through the complexing sites resulting to the production of a vacant site, subsequently reorienting to take up the vacant site [52]. Eq. (5) was employed to compute the CS:MC:NH_4I:glycerol systems DC conductivity at ambient temperature. The DC conductivities of the films are listed in Table 1. It is worth to note that the DC conductivity was improved with increasing glycerol content. Earlier reports have established that polymer electrolytes with high DC conductivity in the range between 10^{-5} and $10^{-3}\,S\,cm^{-1}$ can be employed for applications in electrochemical devices, such as batteries and EDLCs [7,54,55].

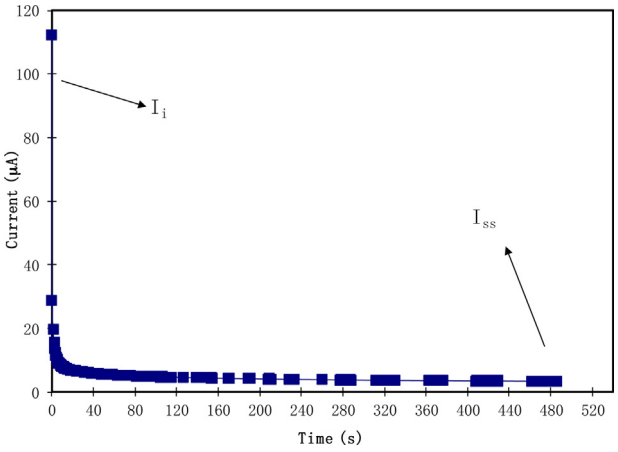

Fig. 5 – Polarization of SS|CSMC4 electrolyte| SS at 0.2 V.

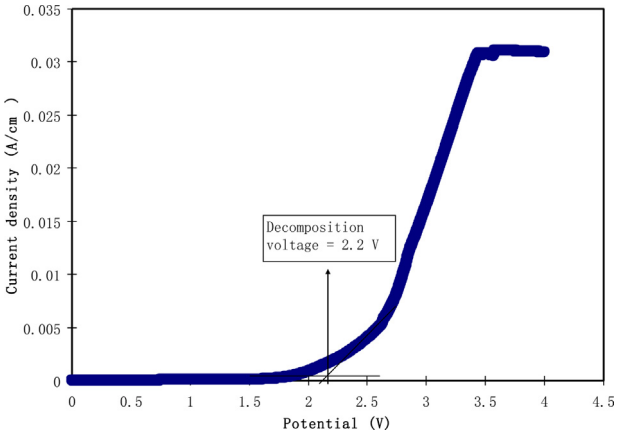

Fig. 6 – Influence of potential on current density through LSV analysis.

3.3. *Electrochemical characteristics*

3.3.1. *TNM study*

Commonly in polymer electrolyte system, there are two charge carriers, electrons and ions. In order to identify which one is the main charge carrier, TNM analysis has been conducted. The use of stainless steel is due to their ionic-blocking effect, thus t_e can be estimated. The polarization process in Fig. 5 shows that the initial current value is quite large (112.2 μA). This is before ions are blocked at the surface of the electrodes. As ions are blocked on the surface of electrodes, the value of the current drops drastically. A steady-state process can be observed at ~50 s where it stabilized at 3.1 μA up to 500 s. This signifies that the electrolyte in this study is an ionic conductor [56].

Using Eq. (1), value of t_{ion} is found to be 0.97, which is approaching 1, while 0.03 for t_e. As $t_{ion} > t_e$, ions are verified to be the main charge carriers to the total conductivity. Thus, the highest conducting electrolyte in this work is suitable to be used in EDLC application, as ions will form electromotive force with carbon electrodes. As reported in our previous work [33], CS:MC:NH_4I system possesses t_{ion} of 0.934, lower than that of CS:MC:NH_4I:glycerol (this work). Thus, the addition of glycerol has enhanced carrier concentration. As stated earlier in the introduction, glycerol has a high dielectric constant, which promotes dissociation of ions. t_{ion} will be enhanced when more free ions are available for conduction process. As reported by Vijaya et al. [57], the t_{ion} for ammonium salt-based electrolytes is in the range between 0.93 and 0.97.

3.3.2. *LSV study*

Electrolyte is used as electrodes separator and will be subjected to a continuous process of rapid charge–discharge. During charging process, a high voltage will be produced and the electrolyte film will breakdown. Thus, it is crucial to examine the potential stability of the electrolyte before any application. From Fig. 6, we can see that there are no obvious changes in current value from 0 V to ~1.7 V. Beyond 1.7 V, current starts to increase slowly. The decomposition voltage is taken at the meeting point between the line of stable current with the line where the current increases sharply. The decomposition voltage of the highest conducting electrolyte (CSMC4) in this study is 2.2 V. The decomposition of CS:MC:NH_4I with the presence of the glycerol is 2.1 V, which is reported in our previous work [33]. Asmara et al. [58] reported that concentration of charge carrier affects the decomposition voltage. This could be due to the increment in charge carrier density

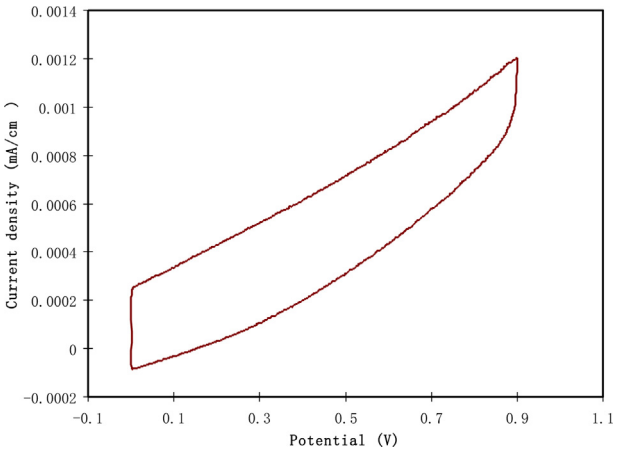

Fig. 7 – Cyclic voltammetry plot for the fabricated EDLC.

with the addition of glycerol. The authors also reported that an EDLC where they charged and discharged to 0.85 V and 0 V, respectively, even though the electrolyte is stable up to 2.42 V. According to the work reported by Shuhaimi [59], the EDLC is only charged up to 0.85 V despite the electrolyte of MC-NH_4NO_3-Poly(ethylene glycol) (PEG) has high decomposition voltage of 2.4 V. The EDLC cannot be charged higher than 0.9 V could be due to electrode's material used.

3.3.3. *CV study*

As the energy storage mechanism of an EDLC is through capacitive process or charge double-layer development, CV analysis is used to confirm this fact. Fig. 7 depicts the CV plot of the EDLC at 0.01 V up to 0.9 V. The shape of the CV plot is nearly a rectangular shape. The divergence of CV plot shape is due to internal resistance as well as porosity of activated carbon electrodes [60]. Furthermore, there are no peaks in the plot meaning that there are no oxidations or reductions happen at the electrodes. It is just electromotive force between ions of the electrolyte and the carbon electrodes [61]. According to Kant et al. [62], a good CV curve signifies excellent charge transportation.

The calculated value of C_{cv} using Eq. (2) is found to be 9.97 F g^{-1}. This value will be compared to the one obtain from charge–discharge analysis later on. Abouimrane et al. [63] reported an activated carbon-based EDLC with tetrabutylammonium hexafluorophosphate salt, $(C_4H_9)_4$-NPF_6, that achieved 7–8 F g^{-1} from CV analysis. An EDLC with carbon aerogel electrodes possessed C_{cv} from 3.31 to 6.43 F g^{-1} [64]. Carbon aerogel has lower surface area (400–1100 m^2 g^{-1}) compared to activated carbon (500–2500 m^2 g^{-1}). Larger surface area provides more electrosorption of NH_4^+ and I^- ions, thus providing higher capacitance. Porosity of the electrode also plays an important role to provide higher capacitance. Heimbockel et al. [65] reported that the capacitance increased as the pore size increased. Activated carbon possesses quite large pore size ranging from 10 to 200 Å. Large pore size enables more solvated ions to enter and undergo adsorption process.

3.4. *Device study*

3.4.1. *Charge–discharge study*

Rechargeability of the EDLC is tested for 100 cycles at 0.4 mA cm^{-2}, as shown in Fig. 8. Ideal charge–discharge curve is like a triangle shape, however due to carbon roughness, electrolyte and internal resistance, the shape diverges. The linearity of discharge part portrays that the mechanism is purely electrostatic interactions between the charged pore surface and the ions rather than redox reaction [66].

By replacing the value of discharge gradient in Eq. (3), the value of specific capacitance from charge–discharge (C_{cd}) will be obtained.

Fig. 9 shows the specific capacitance and equivalent series resistance versus cycle number. Fig. 9a illustrates C_{cd} versus cycle number for 100 cycles. The value of C_{cd} at the 1st cycle is 9.70 F g^{-1}. This result is close the one that obtained from CV, which is 9.97 F g^{-1}. Thus, the value of the capacitance for this EDLC is reliable. However, it drops to 7.13 F g^{-1} at 20th cycle. This could be due to two possible explanations: (i) some charges are consumed in an irreversible process with loosely bound ions, such as OH^- groups, adsorbed onto the surface of the electrodes or (ii) some pores of the activated carbon electrode are blocked permanently during rapid

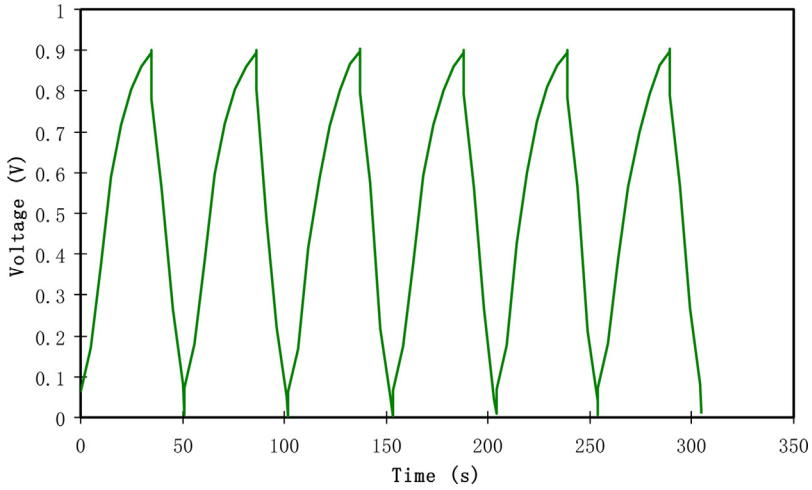

Fig. 8 – Charge–discharge profile of the EDLC at selected cycles.

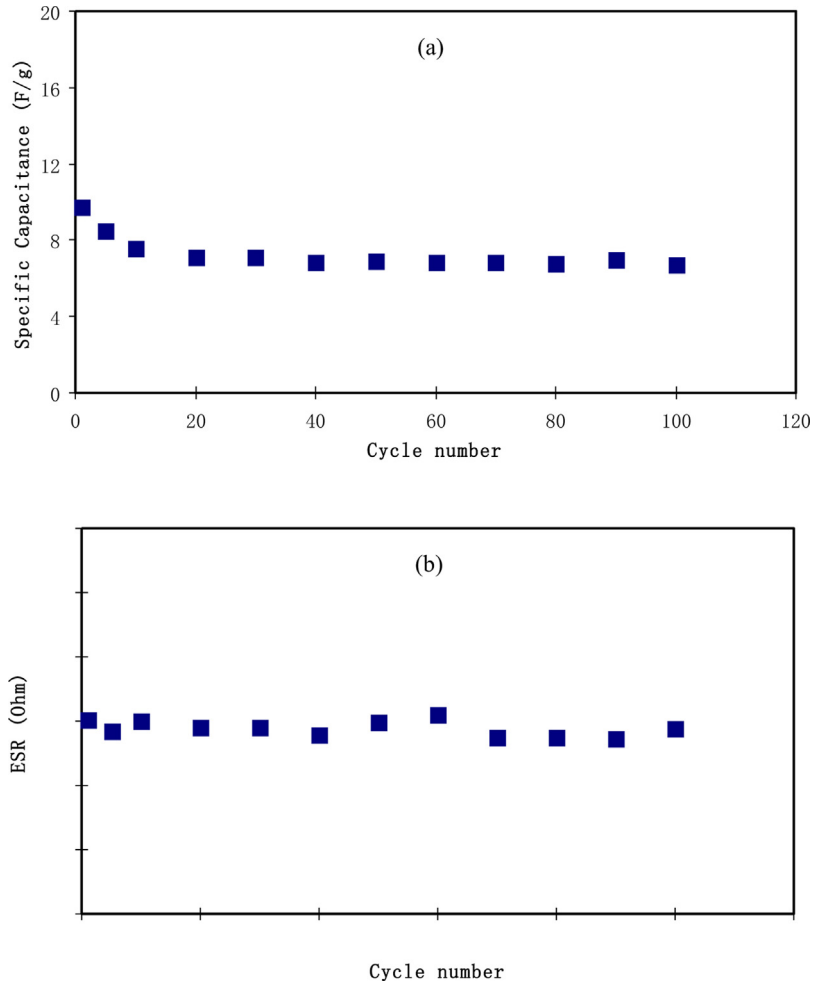

Fig. 9 – The EDLC parameters of (a) specific capacitance and (b) ESR from 1st to 100th cycle at 0.4 mA cm^{-2}.

charge–discharge process [67]. The stabilization of capacitive process can be seen from 30th cycle to 100th cycle with average of 6.90 F g^{-1}. This result is higher compared with that of CS:MC:NH_4I in our previous report [33]. The pattern of the C_{cd} versus cycle number for the CS:MC:NH_4I system in our previous work [33] is similar to this work, where C_{cd} at the 1st cycle is 2.36 F g^{-1} and stabilized at 1.76 F g^{-1}. The presence of glycerol provides alternative pathway for ionic migration due to its OH group in their structure. Ions are easier to move in plasticized electrolyte compared to unplasticized electrolyte. Other than that, plasticizer enhanced the free ion density. Consequently, DC conductivity becomes high which is an important criterion for application of polymer electrolytes in electrochemical devices. Previous studies indicated the non-suitability of low ion conducting (10^{-5} to 10^{-9} S cm^{-1}) polymer electrolytes for electrochemical device applications [13,68]. These two conditions promote more free ions at the surface of the electrodes, consequently improving the specific capacitance.

The values of the specific capacitance obtained in the present work are higher than those in the earlier reports. For instance, Liew et al. [69] documented that the EDLC specific capacitance using PVA:ammonium acetate (CH_3COONH_4) salt possesses specific capacitance of 0.13 F g^{-1} throughout 500 cycles. As documented by Hashmi et al. [55], PEO_9-lithium trifluoromethane sulfonate ($LiCF_3SO_3$)-poly(ethylene glycol) (PEG)200 plasticizer when applied in an EDLC provides small specific capacitance of 4 F g^{-1}.

As observed in Fig. 8, there is a sudden reduction in potential value before discharging process occurs. This is due to the presence of charge transfer resistance, electrolyte and gap between electrode and electrolyte [70]. The calculated value of ESR using Eq. (4) fluctuated from 136 Ω to 155 Ω as shown in Fig. 9b. The changes are not so drastic and can be considered stable. Low ESR displays that the EDLC possesses good electrode–electrolyte interfacial contact, allowing easier electrostatic process between ions and charged electrode [71]. The ESR of the CS:MC:NH_4I electrolyte system without glycerol in our previous work possesses higher ESR value (650–1000 Ω) than the plasticized system in this work [33]. More free ions in plasticized electrolyte can contribute in the double layer development, which could result in lower charge transfer resistance [72]. The ESR obtained in the current work is small compared to the previous reports [52,73].

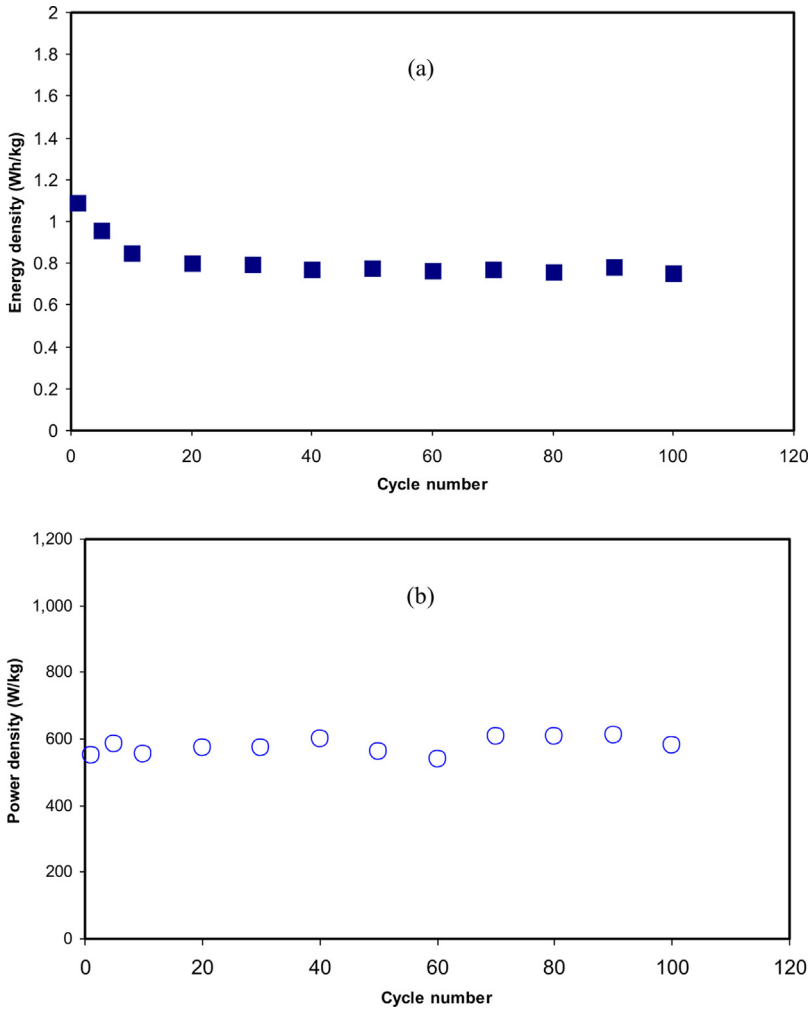

Fig. 10 – The EDLC parameters of (a) energy density and (b) power density from 1st to 100th cycle at 0.4 mA cm^{-2}.

Other important parameters of EDLC such as energy (E_d) and power (P_d) density are calculated using Eqs. (7) and (8) [33]:

$$E_d = \frac{C_s V}{2} \tag{7}$$

$$P_d = \frac{V^2}{4mR_{esr}} \tag{8}$$

where V is applied voltage (0.9 V). Fig. 10 shows the energy (E_d) density and power density (P_d) versus cycle number. Fig. 10a shows the trend of E_d for 100 cycles. It is similar to the trend of C_{cd} in Fig. 9a, where E_d drops from 1.1 Wh kg^{-1} to 0.8 Wh kg^{-1} from 1st to 20th cycle. The constant value of energy density from 30th cycle to 100th cycle (average = 0.77 Wh kg^{-1}) signifies that cations or anions face the same energy barrier during migration toward the surface of the electrode. Liew et al. [74] reported that the E_d of the EDLC with starch/$LiPF_6$/$BmImPF_6$ being stabilized at ~0.41–0.55 Wh kg^{-1}, which is lower than the current work. According to Ragone plot [75], the range of energy density of supercapacitors is changes from 0.05 to 20 Wh kg^{-1}. Power density (P_d) is how much energy can be delivered per kilogram. The P_d of the EDLC can be seen in Fig. 10b where is almost constant up to 100th cycle with average of 578.55 W kg^{-1}. The pattern of P_d is similar with ESR because the ESR affects the value of the P_d. High ESR value means that the gap between electrode and electrolyte is not good thus energy cannot be delivered efficiently [76]. Based on the Ragone plot [75], supercapacitors may have high power density even up to 10^6 W kg^{-1}. Ragone plot is crucial to understand and distinguish between supercapacitors and fuel cells. This plot explains that the fuel cells are high-energy systems; whereas supercapacitors are high-power density systems. The power density gained in the present work is of the great interest compared to the power density of 156.51 W kg^{-1} that gained for EDLC of the corn starch-lithium acetate (LiOAc)-glycerol system [77].

4. Conclusion

Plasticized chitosan (CS):methylcellulose (MC):NH_4I based solid polymer blend electrolytes were prepared fruitfully using solution cast technique. The structural examination reveals the dominance of amorphous phase through the decreasing intensity in the XRD spectrum. The bulk resistance decreased

upon increasing of glycerol plasticizer. The maximum DC ionic conductivity was obtained to be 6.65×10^{-4} S cm^{-1} for the plasticized CS:MC doped with 40 wt% of NH_4I. The highest conducting electrolyte was found to be electrochemically stable up to 2.2 V. Ions were the main charge carriers in the total conductivity as from TNM analysis, it was found that $t_{ion} > t_e$. The specific capacitance for CV and charge–discharge were 9.97 F g^{-1} and 9.70 F g^{-1}, respectively. Thus, EDLC in the current study can be considered to be reliable. Other crucial EDLC parameters have been obtained, e.g. internal resistance (136–155 Ω), energy density (1.1 Wh kg^{-1}) and power density (578.55 W kg^{-1}). The performance of the EDLC was much better with the presence of glycerol in the electrolyte system. Glycerol promotes more salt dissociation as well as creating extra coordinating site for ions to be conducted.

Conflicts of interest

The authors declare no conflict of interest.

Acknowledgments

The authors gratefully acknowledge the financial support for this study from the Ministry of Higher Education and Scientific Research-Kurdish National Research Council (KNRC), Kurdistan Regional Government/Iraq. The financial support from the University of Sulaimani and Komar Research Center (KRC) and Komar University of Science and Technology are greatly appreciated.

REFERENCES

[1] Ansari SA, Parveen N, Han TH, Ansari MO, Cho MH. Fibrous polyaniline@manganese oxide nanocomposites as supercapacitor electrode materials and cathode catalysts for improved power production in microbial fuel cells. Phys Chem Chem Phys 2016;18:9053–60, http://dx.doi.org/10.1039/c6cp00159a.

[2] Han L, Huang H, Fu X, Li J, Yang Z, Liu X, et al. A flexible, high-voltage and safe zwitterionic natural polymer hydrogel electrolyte for high-energy-density zinc-ion hybrid supercapacitor. Chem Eng J 2020;392:123733, http://dx.doi.org/10.1016/j.cej.2019.123733.

[3] Piana G, Bella F, Geobaldo F, Meligrana G, Gerbaldi C. PEO/LAGP hybrid solid polymer electrolytes for ambient temperature lithium batteries by solvent-free, “one pot” preparation. J Energy Storage 2019;26:100947, http://dx.doi.org/10.1016/j.est.2019.100947.

[4] Falco M, Simari C, Ferrara C, Nair JR, Meligrana G, Bella F, et al. Understanding the effect of UV-induced cross-linking on the physicochemical properties of highly performing PEO/LiTFSI-based polymer electrolytes. Langmuir 2019;35:8210–9, http://dx.doi.org/10.1021/acs.langmuir.9b00041.

[5] Falco M, Castro L, Nair JR, Bella F, Bardé F, Meligrana G, et al. UV-cross-linked composite polymer electrolyte for high-rate, ambient temperature lithium batteries. ACS Appl Energy Mater 2019;2:1600–7, http://dx.doi.org/10.1021/acsaem.8b02185.

[6] Scalia A, Bella F, Lamberti A, Gerbaldi C, Tresso E. Innovative multipolymer electrolyte membrane designed by oxygen inhibited UV-crosslinking enables solid-state in plane integration of energy conversion and storage devices. Energy 2019;166:789–95, http://dx.doi.org/10.1016/j.energy.2018.10.162.

[7] Aziz SB, Brza MA, Hamsan MH, Kadir MFZ, Muzakir SK, Abdulwahid RT. Effect of ohmic-drop on electrochemical performance of EDLC fabricated from PVA: dextran:NH_4I based polymer blend electrolytes. J Mater Res Technol 2020;9:3734–45, http://dx.doi.org/10.1016/j.jmrt.2020.01.110.

[8] Aziz SB, Brza MA, Mishra K, Hamsan MH, Karim WO, Abdullah RM, et al. Fabrication of high performance energy storage EDLC device from proton conducting methylcellulose: dextran polymer blend electrolytes. J Mater Res Technol 2019;9:1137–50, http://dx.doi.org/10.1016/j.jmrt.2019.11.042.

[9] Yan C, Jin M, Pan X, Ma L, Ma X. A flexible polyelectrolyte-based gel polymer electrolyte for high-performance all-solid-state supercapacitor application. RSC Adv 2020;10:9299–308, http://dx.doi.org/10.1039/c9ra10701k.

[10] Zhou K, Ma W, Zeng Z, Ma X, Xu X, Guo Y, et al. Experimental and DFT study on the adsorption of VOCs on activated carbon/metal oxides composites. Chem Eng J 2019;372:1122–33, http://dx.doi.org/10.1016/j.cej.2019.04.218.

[11] Nair JR, Colò F, Kazzazi A, Moreno M, Bresser D, Lin R, et al. Room temperature ionic liquid (RTIL)-based electrolyte cocktails for safe, high working potential Li-based polymer batteries, J. Power Sources 2019;412:398–407, http://dx.doi.org/10.1016/j.jpowsour.2018.11.061.

[12] Aziz SB, Brza MA, Saed SR, Hamsan MH, Kadir MFZ. Ion association as a main shortcoming in polymer blend electrolytes based on CS:PS incorporated with various amounts of ammonium tetrafluoroborate. J Mater Res Technol 2020;9:5410–21, http://dx.doi.org/10.1016/j.jmrt.2020.03.067.

[13] Aziz SB, Karim WO, Ghareeb HO. The deficiency of chitosan:$AgNO_3$ polymer electrolyte incorporated with titanium dioxide filler for device fabrication and membrane separation technology. J Mater Res Technol 2020;9:4692–705, http://dx.doi.org/10.1016/j.jmrt.2020.02.097.

[14] Koksbang R, Olsen II, Shackle D. Review of hybrid polymer electrolytes and rechargeable lithium batteries. Solid State Ionics 1994;69:320–35, http://dx.doi.org/10.1016/0167-2738(94)90420-0.

[15] Hirankumar G, Mehta N. Effect of incorporation of different plasticizers on structural and ion transport properties of PVA-$LiClO_4$ based electrolytes. Heliyon 2018;4:e00992, http://dx.doi.org/10.1016/j.heliyon.2018.e00992.

[16] Perd’ochová D, Tomanová K, Alexy P, Bočkaj J, Feranc J, Plavec R, et al. The influence of additives on crystallization of blends based on polylactid acid. IOP Conf Ser Mater Sci Eng 2017;266, http://dx.doi.org/10.1088/1757-899X/266/1/012014.

[17] Mathew CM, Karthika B, Ulaganathan M, Rajendran S. Electrochemical analysis on poly (ethyl methacrylate)-based electrolyte. Bull Mater Sci 2015;38:151–6, http://dx.doi.org/10.1007/s12034-014-0821-8.

[18] Pradima J, Kulkarni MR, Archna. Review on enzymatic synthesis of value added products of glycerol, a by-product derived from biodiesel production, Resour. Technol 2017;3:394–405, http://dx.doi.org/10.1016/j.reffit.2017.02.009.

[19] Chai MN, Isa MIN. Novel proton conducting solid bio-polymer electrolytes based on carboxymethyl cellulose doped with oleic acid and plasticized with glycerol. Sci Rep 2016;6:27328, http://dx.doi.org/10.1038/srep27328.

[20] Antognini A, Nez F, Schuhmann K, Amaro FD, Biraben F, Cardoso JMR, et al. Proton structure from the measurement of 2S-2P transition frequencies of muonic hydrogen. Science 2013;339:417–20, http://dx.doi.org/10.1126/science.1230016.

[21] Rosi M, Iskandar F, Abdullah M. Hydrogel-polymer electrolytes based on polyvinyl alcohol and hydroxyethylcellulose for supercapacitor applications. Int J Electrochem Sci 2014;9:4251–6.
[22] Łatoszyńska AA, Zukowska GZ, Rutkowska IA, Taberna PL, Simon P, Kulesza PJ, et al. Non-aqueous gel polymer electrolyte with phosphoric acid ester and its application for quasi solid-state supercapacitors. J Power Sources 2015;274:1147–54, http://dx.doi.org/10.1016/j.jpowsour.2014.10.094.
[23] Justin Raj C, Varma KBR. Synthesis and electrical properties of the (PVA)0.7(KI) $0.3{\cdot}_{x}H_2SO_4$ ($0 \leq x \leq 5$) polymer electrolytes and their performance in a primary Zn/MnO_2 battery. Electrochim Acta 2010;56:649–56, http://dx.doi.org/10.1016/j.electacta.2010.09.076.
[24] Khiar ASA, Arof AK. Conductivity studies of starch-based polymer electrolytes. Ionics (Kiel) 2010;16:123–9, http://dx.doi.org/10.1007/s11581-009-0356-y.
[25] Hassan MF, Zainuddin SK, Kamarudin KH, Sheng CK, Adha Abdullah MA. Ion-conducting polymer electrolyte films based on poly (sodium 4-styrenesulfonate) complexed with ammonium nitrate: studies based on morphology, structural and electrical spectroscopy. Malaysian J Anal Sci 2018;22:238–48, http://dx.doi.org/10.17576/mjas-2018-2202-08.
[26] Hemalatha R, Alagar M, Selvasekarapandian S, Sundaresan B, Moniha V. Studies of proton conducting polymer electrolyte based on PVA, amino acid proline and NH4SCN, J. Sci Adv Mater Devices 2019;4:101–10, http://dx.doi.org/10.1016/j.jsamd.2019.01.004.
[27] Shuhaimi NEA, Alias NA, Majid SR, Arof AK. Electrical double layer capacitor with proton conducting κ-carrageenan chitosan electrolytes. Funct Mater Lett 2008;1:195–201, http://dx.doi.org/10.1142/S1793604708000423.
[28] Anuar NK, Zainal N, Mohamed NS, Subban RHY. Studies of poly(ethyl methacrylate) complexed with ammonium trifluoromethanesulfonate. Adv Mater Res 2012;501:19–23, http://dx.doi.org/10.4028/www.scientific.net/AMR.501.19.
[29] Abbas Q, Raza R, Shabbir I, Olabi AG. Heteroatom doped high porosity carbon nanomaterials as electrodes for energy storage in electrochemical capacitors: a review. J Sci Adv Mater Devices 2019;4:341–52, http://dx.doi.org/10.1016/j.jsamd.2019.07.007.
[30] Machrouhi A, Alilou H, Farnane M, El Hamidi S, Sadiq M, Abdennouri M, et al. Statistical optimization of activated carbon from Thapsia transtagana stems and dyes removal efficiency using central composite design. J Sci Adv Mater Devices 2019;4:544–53, http://dx.doi.org/10.1016/j.jsamd.2019.09.002.
[31] Zhao XY, Wu Y, Cao JP, Zhuang QQ, Wan X, He S, et al. Preparation and characterization of activated carbons from oxygen-rich lignite for electric double-layer capacitor. Int J Electrochem Sci 2018;13:2800–16, http://dx.doi.org/10.20964/2018.03.50.
[32] Buraidah MH, Arof AK. Characterization of chitosan/PVA blended electrolyte doped with NH_4I. J Non Cryst Solids 2011;357:3261–6, http://dx.doi.org/10.1016/j.jnoncrysol.2011.05.021.
[33] Aziz SB, Hamsan MH, Abdullah RM, Abdulwahid RT, Brza MA, Marif AS, et al. Protonic EDLC cell based on chitosan (CS): methylcellulose (MC) solid polymer blend electrolytes. Ionics (Kiel) 2020;26:1829–40, http://dx.doi.org/10.1007/s11581-020-03498-5.
[34] Liu PT, Wei XM, Liu Z. Miscibility study of chitosan and methylcellulose blends. Adv Mater Res 2013;750–752:802–5, http://dx.doi.org/10.4028/www.scientific.net/AMR.750-752.802.
[35] Nik Aziz NA, Idris NK, Isa MIN. Solid polymer electrolytes based on methylcellulose: FT-IR and ionic conductivity studies. Int J Polym Anal Charact 2010;15:319–27, http://dx.doi.org/10.1080/1023666X. 2010.493291.
[36] Aziz SB, Rasheed MA, Ahmed HM. Synthesis of polymer nanocomposites based on [methyl cellulose](1−x):(CuS)x ($0.02\,M \leq x \leq 0.08\,M$) with desired optical band gaps. Polymers (Basel) 2017;9:194, http://dx.doi.org/10.3390/polym9060194.
[37] Aziz SB, Kadir MFZ, Abidin ZHZ. Structural, morphological and electrochemical impedance study of CS: LiTf based solid polymer electrolyte: reformulated arrhenius equation for ion transport study. Int J Electrochem Sci 2016;11:9228–44, http://dx.doi.org/10.20964/2016.11.18.
[38] Aziz SB, Abdullah RM. Crystalline and amorphous phase identification from the tanδ relaxation peaks and impedance plots in polymer blend electrolytes based on [CS:AgNt]x:PEO(x−1) ($10 \leq x \leq 50$). Electrochim Acta 2018;285:30–46, http://dx.doi.org/10.1016/j.electacta.2018.07.233.
[39] Göktepe F, Çelik SÜ, Bozkurt A. Preparation and the proton conductivity of chitosan/poly(vinyl phosphonic acid) complex polymer electrolytes. J Non Cryst Solids 2008;354:3637–42, http://dx.doi.org/10.1016/j.jnoncrysol.2008.03.023.
[40] Aziz SB, Abidin ZHZ, Kadir MFZ. Innovative method to avoid the reduction of silver ions to silver nanoparticles (Ag^{+}-Ag0) in silver ion conducting based polymer electrolytes. Phys Scr 2015;90:35808, http://dx.doi.org/10.1088/0031-8949/90/3/035808.
[41] Wan Y, Creber KAM, Peppley B, Tam Bui V. Chitosan-based solid electrolyte composite membranes: I. Preparation and characterization. J Membr Sci 2006;280:666–74, http://dx.doi.org/10.1016/j.memsci.2006.02.024.
[42] Aziz SB. Role of dielectric constant on ion transport: reformulated Arrhenius equation. Adv Mater Sci Eng 2016;2016:1, http://dx.doi.org/10.1155/2016/2527013.
[43] Aziz SB, Abidin ZHZ, Arof AK. Effect of silver nanoparticles on the DC conductivity in chitosan–silver triflate polymer electrolyte. Phys B Condens Matter 2010;405:4429–33, http://dx.doi.org/10.1016/j.physb.2010.08.008.
[44] Sequeira CAC, Plancha MJC, Araujo LPS. Conductivity studies on solid polymer electrolytes. J Phys IV JP 1994;4:17–35, http://dx.doi.org/10.1051/jp4:1994102.
[45] Aziz SB, Woo TJ, Kadir MFZ, Ahmed HM. A conceptual review on polymer electrolytes and ion transport models. J Sci Adv Mater Devices 2018;3:1–17, http://dx.doi.org/10.1016/j.jsamd.2018.01.002.
[46] Polu AR, Kumar R. AC impedance and dielectric spectroscopic studies of Mg^{2+} ion conducting PVA-PEG blended polymer electrolytes. Bull Mater Sci 2011;34:1063–7, http://dx.doi.org/10.1007/s12034-011-0132-2.
[47] Zhang S, Yang L, Liu Q. Impedance study on the interface of poly electrolyte and metal sodium. Solid State Ionics 1995;76:127–32, http://dx.doi.org/10.1016/0167-2738(94)00239-O.
[48] Benedict TJ, Banumathi S, Veluchamy A, Gangadharan R, Ahamad AZ, Rajendran S. Characterization of plasticized solid polymer electrolyte by XRD and AC impedance methods. J Power Sources 1998;75:171–4, http://dx.doi.org/10.1016/S0378-7753(98)00063-9.
[49] Aziz SB, Abidin ZHZ, Arof AK. Influence of silver ion reduction on electrical modulus parameters of solid polymer electrolyte based on chitosan–silver triflate electrolyte membrane. Express Polym Lett 2010;4:300–10, http://dx.doi.org/10.3144/expresspolymlett.2010.38.
[50] Aziz SB, Abdullah RM, Rasheed MA, Ahmed HM. Role of ion dissociation on DC conductivity and silver nanoparticle formation in PVA:AgNt based polymer electrolytes: deep insights to ion transport mechanism. Polymers (Basel) 2017;9:338, http://dx.doi.org/10.3390/polym9080338.

[51] Hamsan MH, Shukur MF, Kadir MFZ. The effect of NH_4NO_3 towards the conductivity enhancement and electrical behavior in methyl cellulose-starch blend based ionic conductors. Ionics (Kiel) 2017;23:1137–54, http://dx.doi.org/10.1007/s11581-016-1918-4.
[52] Samsudin AS, Isa MIN. Characterization of carboxy methylcellulose doped with DTAB as new types of biopolymer electrolytes. Bull Mater Sci 2012;35:1123–31, http://dx.doi.org/10.1007/s12034-012-0396-1.
[53] Aziz SB, Karim WO, Qadir KW, Zafar Q. Proton ion conducting solid polymer electrolytes based on chitosan incorporated with various amounts of barium titanate (BaTiO3). Int J Electrochem Sci 2018;13:6112–25, http://dx.doi.org/10.20964/2018.06.38.
[54] Lim CS, Teoh KH, Liew CW, Ramesh S. Capacitive behavior studies on electrical double layer capacitor using poly (vinyl alcohol)-lithium perchlorate based polymer electrolyte incorporated with TiO_2. Mater Chem Phys 2014;143:661–7, http://dx.doi.org/10.1016/j.matchemphys.2013.09.051.
[55] Hashmi SA, Latham RJ, Linford RG, Schlindwein WS. Studies on all solid state electric double layer capacitors using proton and lithium ion conducting polymer electrolytes. J Chem Soc Faraday Trans 1997;93:4177–82, http://dx.doi.org/10.1039/a704661h.
[56] Diederichsen KM, McShane EJ, McCloskey BD. Promising routes to a high Li^+ transference number electrolyte for lithium ion batteries. ACS Energy Lett 2017;2:2563–75, http://dx.doi.org/10.1021/acsenergylett.7b00792.
[57] Vijaya NVN, Selvasekarapandian SSS, Malathi JMJ, Iwai YIY, Nithya HNH, Kawamura JKJ. ^{1}H NMR study on PVP-NH4Cl based-proton conducting polymer electrolyte. Indian J Appl Res 2011;3:506–10, http://dx.doi.org/10.15373/2249555x/dec2013/154.
[58] Asmara SN, Kufian MZ, Majid SR, Arof AK. Preparation and characterization of magnesium ion gel polymer electrolytes for application in electrical double layer capacitors. Electrochim Acta 2011;57:91–7, http://dx.doi.org/10.1016/j.electacta.2011.06.045.
[59] Shuhaimi NEA. Ionic conductivity and related studies in methyl cellulose based polymer electrolytes and application in supercapacitors. Kuala Lumpur: University of Malaya; 2011 [MSc dissertation].
[60] Pérez-Madrigal MM, Edo MG, Alemán C. Powering the future: application of cellulose-based materials for supercapacitors. Green Chem 2016;18:5930–56, http://dx.doi.org/10.1039/c6gc02086.
[61] Kasprzak D, Stępniak I, Galiński M. Electrodes and hydrogel electrolytes based on cellulose: fabrication and characterization as EDLC components. J Solid State Electrochem 2018;22:3035–47, http://dx.doi.org/10.1007/s10008-018-4015-y.
[62] Kant R, Singh MB. Theory of the electrochemical impedance of mesostructured electrodes embedded with heterogeneous micropores. J Phys Chem C 2017;121:7164–74, http://dx.doi.org/10.1021/acs.jpcc.7b01287.
[63] Abouimrane A, Belharouak I, Abu-Lebdeh YA. An all-solid-state electrochemical double-layer capacitor based on a plastic crystal electrolyte. Front Energy Res 2015;3:1–6, http://dx.doi.org/10.3389/fenrg.2015.00034.
[64] Hou CH, Huang CY, Hu CY. Application of capacitive deionization technology to the removal of sodium chloride from aqueous solutions. Int J Environ Sci Technol 2013;10:753–60, http://dx.doi.org/10.1007/s13762-013-0232-1.
[65] Heimböckel R, Hoffmann F, Fröba M. Insights into the influence of the pore size and surface area of activated carbons on the energy storage of electric double layer capacitors with a new potentially universally applicable capacitor model. Phys Chem Chem Phys 2019;21:3122–33, http://dx.doi.org/10.1039/c8cp06443a.
[66] Cho S, Chen C-F, Mukherjee PP. Influence of microstructure on impedance response in intercalation electrodes. J Electrochem Soc 2015;162:A1202–14, http://dx.doi.org/10.1149/2.0331507jes.
[67] Suleman M, Deraman M, Othman MAR, Omar R, Hashim MA, Basri NH, et al. Electric double-layer capacitors with tea waste derived activated carbon electrodes and plastic crystal based flexible gel polymer electrolytes. J Phys Conf Ser 2016;739, http://dx.doi.org/10.1088/1742-6596/739/1/012086.
[68] Aziz SB, Abdullah RM, Kadir MFZ, Ahmed HM. Non suitability of silver ion conducting polymer electrolytes based on chitosan mediated by barium titanate ($BaTiO_3$) for electrochemical device applications. Electrochim Acta 2019;296:494–507, http://dx.doi.org/10.1016/j.electacta.2018.11.081.
[69] Liew C, Ramesh S, Arof AK. Enhanced capacitance of EDLCs (electrical double layer capacitors) based on ionic liquid-added polymer electrolytes. Energy 2016;109:546–56, http://dx.doi.org/10.1016/j.energy.2016.05.019.
[70] Arof AK, Kufian MZ, Syukur MF, Aziz MF, Abdelrahman AE, Majid SR. Electrical double layer capacitor using poly (methyl methacrylate)–C4BO8Li gel polymer electrolyte and carbonaceous material from shells of mata kucing (Dimocarpus longan) fruit. Electrochim Acta 2012;74:39–45, http://dx.doi.org/10.1016/j.electacta.2012.03.171.
[71] Kwon YH, Kumar S, Bae J, Seo Y. CVD-graphene for low equivalent series resistance in rGO/CVD-graphene/Ni-based supercapacitors. Nanotechnology 2018;29:195404, http://dx.doi.org/10.1088/1361-6528/aab236.
[72] Kang J, Wen J, Jayaram SH, Yu A, Wang X. Development of an equivalent circuit model for electrochemical double layer capacitors (EDLCs) with distinct electrolytes. Electrochim Acta 2014;115:587–98, http://dx.doi.org/10.1016/j.electacta.2013.11.002.
[73] Hamsan MH, Shukur MF, Aziz SB, Yusof YM, Kadir MFZ. Influence of NH_4Br as an ionic source on the structural/electrical properties of dextran-based biopolymer electrolytes and EDLC application. Bull Mater Sci 2020:43, http://dx.doi.org/10.1007/s12034-019-2008-9.
[74] Liew C, Ramesh S. Electrical, structural, thermal and electrochemical properties of corn starch-based biopolymer electrolytes. Carbohydr Polym 2015;124:222–8, http://dx.doi.org/10.1016/j.carbpol.2015.02.024.
[75] Poonam K, Sharma A, Arora SK, Tripathi. Review of supercapacitors: materials and devices. J Energy Storage 2019;21:801–25, http://dx.doi.org/10.1016/j.est.2019.01.010.
[76] Yassine M, Fabris D. Performance of commercially available supercapacitors. Energies 2017;10:26823882, http://dx.doi.org/10.3390/en10091340.
[77] Shukur MF, Ithnin R, Kadir MFZ. Electrical characterization of corn starch-LiOAc electrolytes and application in electrochemical double layer capacitor. Electrochim Acta 2014;136:204–16, http://dx.doi.org/10.1016/j.electacta.2014.05.075.